UNIVERSITY OF SCIENCE AND TECHNOLOGY OF HANOI

------ ✍ ------

INTERNSHIP REPORT

Morphology and kinematics of the CO(3-2) and continuum emissions of the planetary disc 49 Cet

Student's name **: Nguyen Tung Lam**

Major **: SPACE**

Intake **: 2015-2017**

Supervisor **: Dr. Do Thi Hoai**

Laboratory **: Department of Astrophysics – Vietnam National Satellite Center**

HANOI – 2016

ACKNOWLEDGEMENTS

First and foremost, I wish to express my sincerest gratitude to my supervisor, Dr. Do Thi Hoai for her dedicated instructions and helpful advice during the course of research. I also deeply appreciate Prof. Pierre Darriulat, Dr. Pham Tuyet Nhung and other members of the Department of Astrophysics for their careful reviews and valuable comments on my work. Without their support, I would not have finished my internship successfully.

Specially, I would like to acknowledge University of Science and Technology of Hanoi and Vietnam National Satellite Center for facilitating and supporting my internship.

This paper makes use of the following ALMA data: ADS/JAO.ALMA#2012.1.00195.S. ALMA is a partnership of ESO (representing its member states), NSF (USA) and NINS (Japan), together with NRC (Canada) and NSC and ASIAA (Taiwan) and KASI (Republic of Korea), in cooperation with the Republic of Chile. The Joint ALMA Observatory is operated by ESO, AUI/NRAO and NAOJ. I am indebted to and very grateful for the ALMA partnership, who are making their data available to the public after a one year period of exclusive property, an initiative that means invaluable support and encouragement for Vietnamese astrophysics.

TABLE OF CONTENTS

I. INTRODUCTION TO DEPARTMENT OF ASTROPHYSICS – VNSC

The Department of Astrophysics (DAP) was founded at the Vietnam National Satellite Center under the Decision No. 37/QĐ-TTVTQG dated January 29th, 2015. The precursor of DAP was the Vietnam Astrophysics Training Laboratory (VATLY, INST), which was a group of scientists with over 14 years of experience in the field of astrophysics. The Department of Astrophysics consists of 8 members: 1 professor, 5 doctors, 1 master and 1 bachelor, mostly majored in physics.

The goal of the Department is to form a research group of international stature in astrophysics and space sciences in Vietnam. It has the functions of conducting studies in astrophysics and space sciences, building human resources for the fields and performing public outreach and education in order to raise public awareness of the meaning, roles and importance of astrophysics and space sciences in particular and of fundamental research in general.

Achieving excellence in research is the first concern of the Department. The field of research is aimed to be astrophysics in a broad sense, both space and ground based and at any wavelength from radio to gamma rays. However, in the current stage, it focuses on radio astronomy, in which members are proficient. Research in this field involves the utilization of large facilities typically operated at international level, which indicates collaboration with research groups around the world.

At present, the team is collaborating with the Observatoire de Paris on AGB stars and the transition to protoplanetary nebulae and with University of Toulouse on distant galaxies (epoch of maximal star formation). Their goal is to possibly maintain these cooperations while facilitating new ones, which allows extending their study in either the same or new subjects. Specifically, the role of VNSC in the Japan-Vietnam agreement on Research and Development should enable access to ALMA data in collaboration with Japanese teams; the prospect of cooperating with China on FAST, the new radio antenna being built in nearby China is being studied for the purpose of initiating research on pulsars, especially millisecond pulsars. As a general rule, cooperations within the Asia-Pacific region will be specially considered.

The team has published 15 papers in national journals (mostly refereed by international referees), over 60 papers in international scientific journals and many proceeding contributions in national and international conferences. The full list of publications is posted on the DAP's website: http://dap.vnsc.org.vn/ (Vietnam National Satellite Center 2016).

II. RESEARCH WORK

The present report relates work done in DAP in summer 2016 in the context of a 2-month internship. The purpose of the work is to study the morphology and kinematics of the CO(3-2) and continuum emissions of the planetary disc 49 Cet. The disc of 49 Cet is a debris disc, which is likely the site of the last stages of planet formation.

In the following section I describe briefly the general picture of the formation of the star and of the planetary disc. It also provides some details on the debris disc. The second section reviews the main properties of 49 Cet and previous observations of this source. The third section presents the result of our work on the observation of CO(3-2) and continuum emissions obtained by ALMA and its analysis. A short summary is given at the end of the report.

1. Star formation and planetary disc evolution

1.1. Star formation

The general picture of the development of a young, Sun-like star can be summarised as a series of stages that cover about 50 million years (Figure 1). Star formation begins inside dark interstellar clouds containing high-density regions. When the molecular cloud core reaches critical mass, it collapses forming a protostar and a surrounding envelope of gas and dust. The initial angular momentum of the molecular cloud drives the formation of a disc. Material accretes onto the protostar from the disc, which drives a bipolar outflow. When the dusty envelope dissipates, the object becomes visible at optical wavelengths for the first time as a T Tauri star. After a few million years the dusty disc also dissipates, leaving a bare pre-main-sequence star at its centre. In some instances, a debris disc with newly formed planets may continue to orbit the star. The star continues its gravitational collapse to the point where its core temperature becomes hot enough for nuclear fusion, and the object becomes a main-sequence star. Finally a young stellar system is obtained with a central star and planets around.

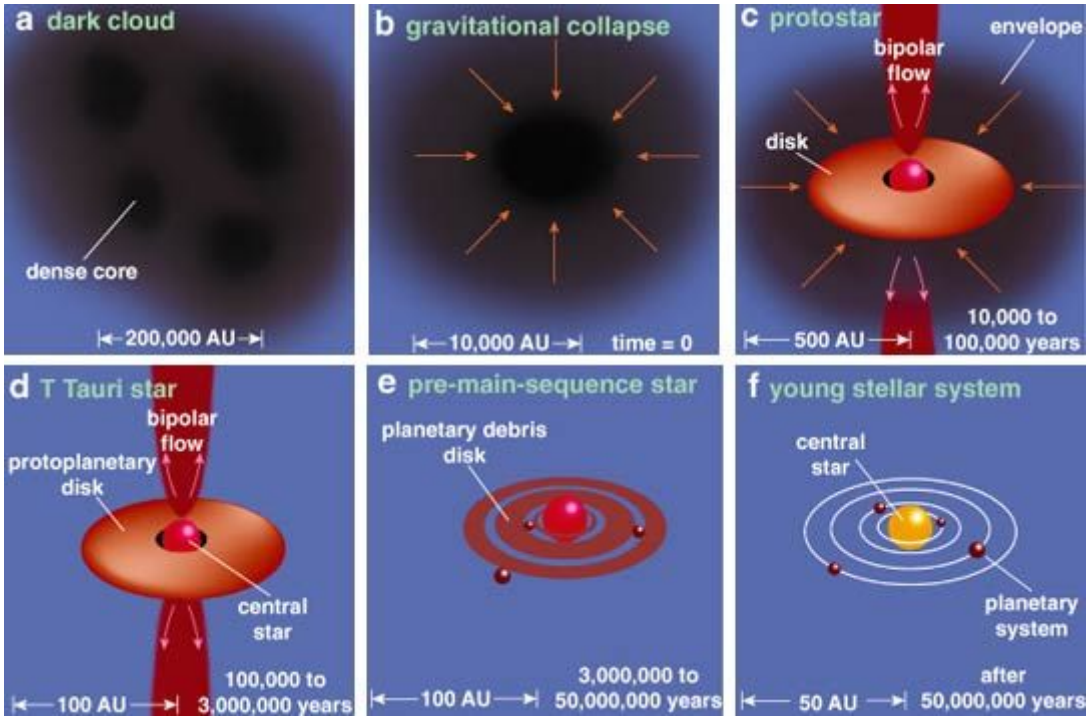

Figure 1. Overview of the star and planet formation process. The sizes and timescales are also presented for the different evolutionary stages (Greene, 2001).

1.2. ***Evolution of a protoplanetary disc***

Although the complex evolution of the planetary disc is not fully understood, the current understanding of the evolution of a typical disc can be summarised as follow (illustrated in Figure 2, see more details in Williams & Cieza, 2011).

Early in its evolution, the disc loses mass through accretion onto the star and FUV photo-evaporation of the outer disc. During this mass depletion stage, which lasts several million years, an object would be classified as a classical T Tauri star based on the presence of accretion indicators (Figure 2a).

Grains grow into larger bodies that settle onto the mid-plane of the disc in the form of rocks, planetesimals... The initially flared dusty disc becomes flatter (Figure 2b). These primordial, or protoplanetary discs, are gas-rich, optically thick discs around pre-main sequence stars.

As disc mass and accretion rate decrease, extreme-UV-induced photo-evaporation becomes important; the outer disc is no longer able to resupply the inner disc with material, and the inner disc drains on a viscous timescale ($\sim 10^5$ years). An inner hole is formed, accretion onto the star ceases, and the disc quickly dissipates from the inside out (Figure 2c). This results in a rapid transition between classical T Tauri star and weak T Tauri star stage. Transitional discs were first classified by a deficit of mid-IR flux in the spectral energy distribution (SED). This dip in the mid-IR corresponds to a

lack of small dust grains in the inner disc. Transitional discs still show large quantities of gas, at least the outer parts.

Once the remaining gas photo-evaporates, the small grains are removed by radiation pressure and Poynting-Robertson drag (meaning that grains having diameters between 1 μm and 1 mm spiral slowly into the star, Figure 2d). Only large grains, planetesimals, and/or planets are left. These debris discs are very low mass and are not always detectable. They are gas-poor and optically thin, with small fractional dust luminosities. They are composed of secondary material recently generated by collisions between and evaporation of asteroids and comets. Small amounts of gas have been detected in several debris discs. The primarily atomic gas must also be recently produced secondary material as many of species seen have short lifetimes in optically-thin environments. As for the dust, the ultimate source of the gas is the destruction of planetesimals (Roberge & Kamp 2011).

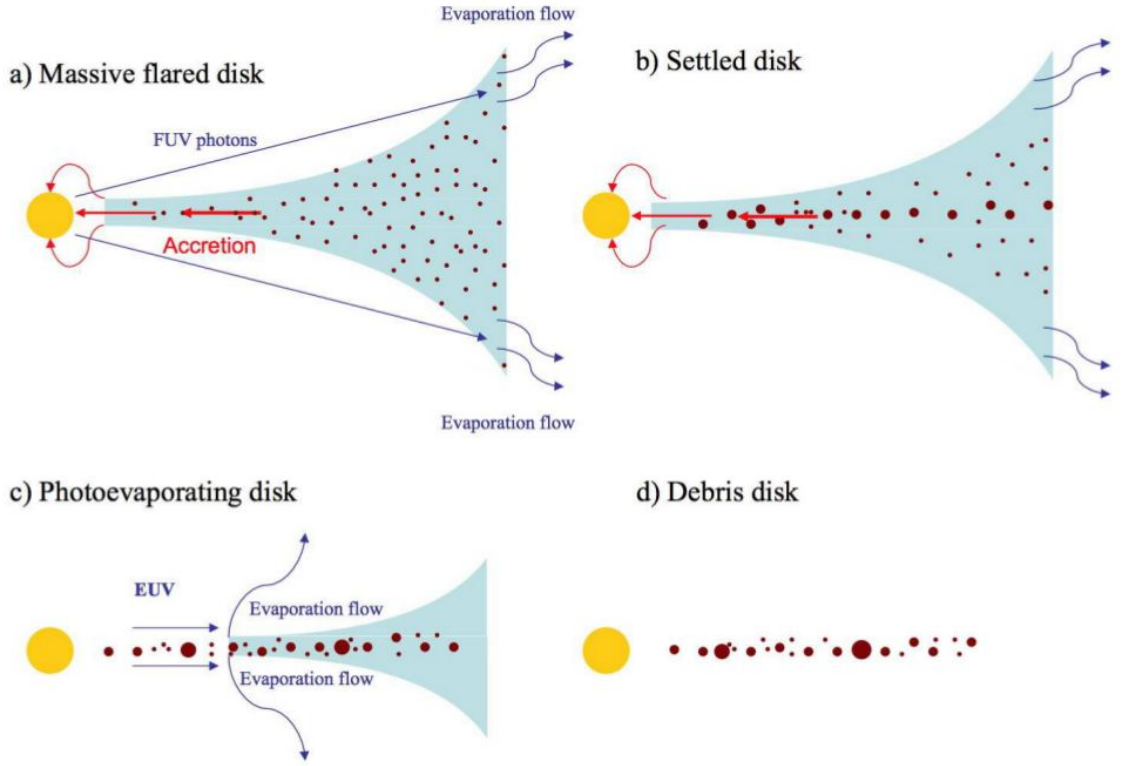

Figure 2. Overview of the evolution of a typical disc. The gas distribution is shown in blue and the dust in red.

2. Overview of 49 Cet

49 Ceti is a main sequence A1V star surrounded by a young debris disc. The distance to the Earth is 59±1 pc (van Leuween 2007). Its low luminosity in infrared ($\tau = L_{IR}/L_{bol} = 8\times10^{-4}$, Rhee et al. 2007) shows that the dust is optically thin. The stellar age is first estimated around 8 Myr by Thi et al. (2001) using the evolutionary tracks of Siess et al. (2000) and its position on the H-R diagram. Then, Zuckerman & Song (2012) demonstrated that 49 Cet

is a member of Argus Association which has an age of ~40 Myr (Torres et al. 2008) based on the Galactic space motions (UVW) and the location on an A-type star colour–magnitude diagram (CMD).

49 Ceti is surrounded by a circumstellar disc which is in debris phase with the presence of two dust rings, an inner warm component and an outer cold component. The spectral energy distribution (SED) of this star is well fitted with the stellar emission and a dust excess emission of two dust rings in thermal equilibrium having temperatures of 175 and 62 K (Figure 3, Roberge et al. 2014). Based on these results and assuming the simple blackbody emitting grains to be in radiative equilibrium, they find lower limits for the locations of the rings, 11 and 84 AU respectively.

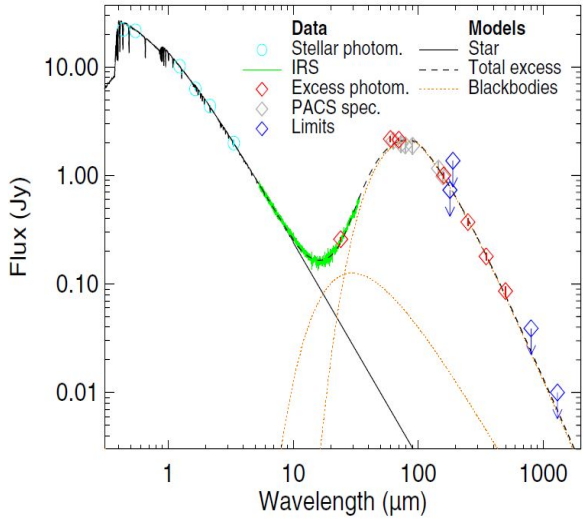

Figure 3. Spectral energy distribution for 49 Cet with a two-component blackbody model for the dust excess emission. The best stellar model (solid black line) was fit to the B and V agnitudes from the Tycho-2 Catalogue, the J, H, and K fluxes from 2MASS, and the WISE W1 flux (cyan circles). The total model (black dashed line) is the sum of the best-fitting stellar model, a warm simple blackbody, and a cold modified blackbody. It is fit to various photometry detections (red diamonds), continuum fluxes from PACS spectroscopy (grey diamonds), and the Spitzer IRS spectrum (green line). The individual blackbody components are plotted with orange dotted lines. Some relevant flux upper limits are also shown (blue arrows).

49 Ceti is one of only three debris discs known to show sub-millimetre CO emission. (Zuckerman et al. 1995; Dent et al. 2005; Hughes et al. 2008); the others are HD 21997 (Moor et al. 2011) and β Pictoris (Dent et al. 2014). The first spatial resolved image was observed by Hughes et al. (2008) in CO(2-1) using the Submillimeter Array with a resolution of 1.0×1.2 arcsec^2 (Figure 4). The observed emission reveals an extended rotating structure viewed approximately edge-on and clear of detectable CO emission out to a distance of 90 AU from the star. Models of disc structure and chemistry indicate that the inner disc is devoid of molecular gas, while the outer gas disc between 40 and 200 AU from the star is dominated by photochemistry from stellar and interstellar radiation.

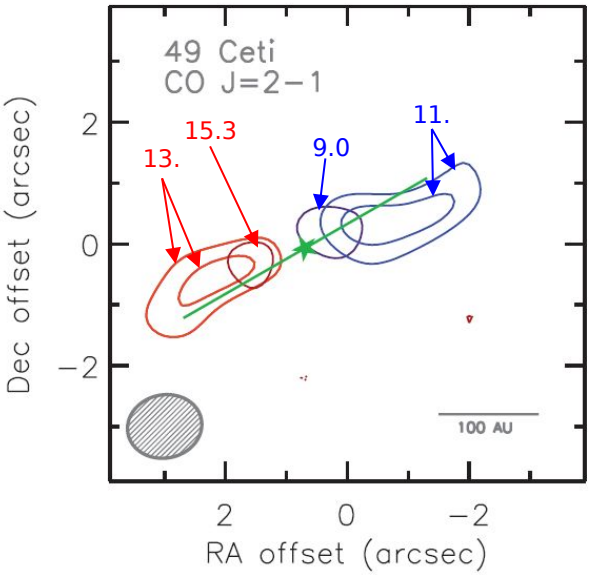

Figure 4. Superposition of 4 CO(2-1) channel maps corresponding to Doppler velocity bins centred on 9.0, 11.1, 13.2, and 15.3 km/s respectively**.** The position of 49 Ceti is marked with a star symbol, while the green line indicates the position angle derived by Wahhaj et al. (2007) from mid-IR imaging. The contour colours indicate the blue shifted (blue) and red shifted (red) velocities.

Observing the dust emission at 70 µm, Roberge et al. (2014) obtained the spatially resolved image of the outer disc for the first time (Figure 5). The agreement in the orientation and location of the 70 µm dust disc and the CO(2-1) disc suggests that the gas and dust are co-spatial. They also detected CII line emission (158 µm) but could not detect OI (63 µm), which is a common emission of planetary discs. This result supports strongly the hypothesis that the origin of the gas is from evaporating comets or colliding planetary material.

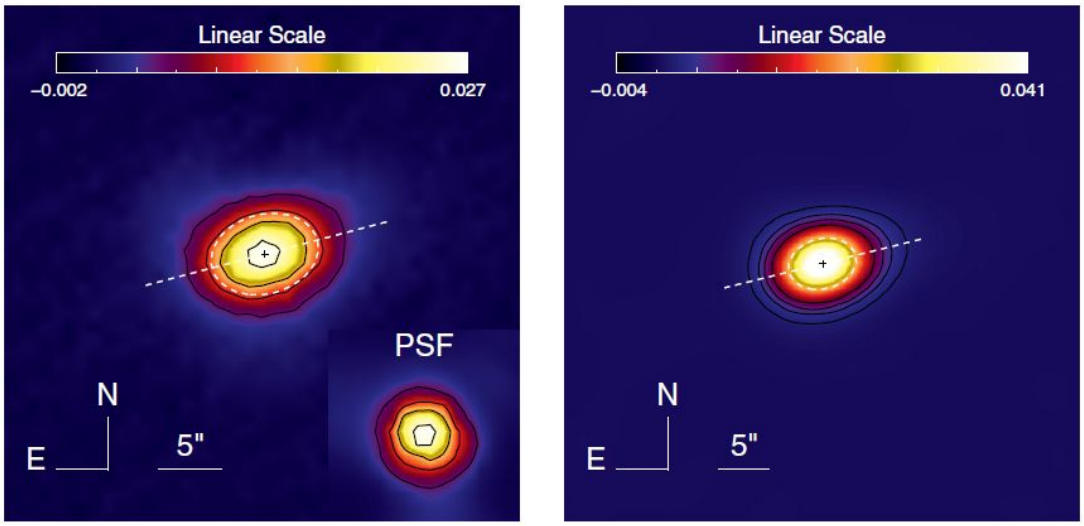

Figure 5. Herschel PACS 70µm images of 49 Cet. The dashed white ellipse shows the half-maximum contour for the best-fitting 2D Gaussian. *Left:* original calibrated scan map with the insert of PSF observation of α Boo in the lower right corner. *Right:*

The map of 49 Ceti after deconvolution using the PSF. The position angle of −76° is shown as a white dashed line

3. ALMA observations of the continuum and CO(3-2) line emission

The emission from 49 Ceti was observed by ALMA on 14th November 2013 (project code: 2012.1.00195.S) during 39 minutes in both continuum (width of 15.016 MHz, from 342.994 to 358.010 GHz) and CO(3-2) line emission. They used 28 antennas with the maximum baseline of 1284.3 m. The data were reduced by ALMA Helpdesk in 2016 and published on JVO portal (http://jvo.nao.ac.jp/portal) under the data set id ALMA01012318 (for line data) and ALMA01012317 (for continuum data).

3.1. *Continuum data*

The continuum data is presented in the grid of 360×360 pixels with the pixel size of 0.1×0.1 arcsec^2. The angular resolution is 0.56×0.43 arcsec^2 with position angle, PA=88.6°. Figure 6 displays the flux density distribution. The Gaussian fit around 0 gives a mean of 5.6×10^{-5} mJy/beam and a σ of 0.055 mJy/beam. We use a cut at 3σ. The total flux of the continuum is 8.1 mJy.

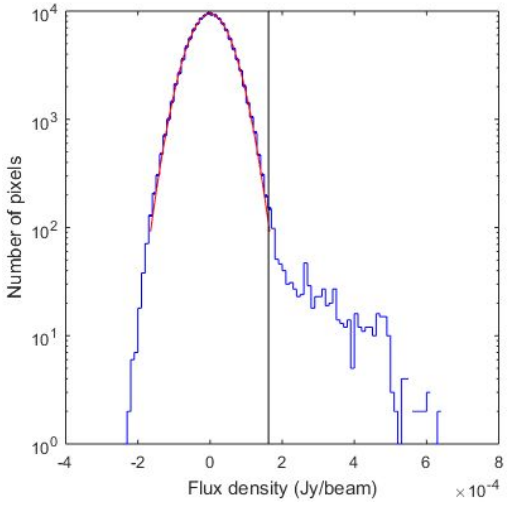

Figure 6. Distributions of the continuum flux density with the Gaussian fit (red curve), the vertical line shows the cut at 3σ

Figure 7 shows the map of flux density and Figure 8 displays its projection on RA and Dec averaged over pixels. The mean values of the *x* and *y* projections are 0.0235 and −0.0028 arcsec respectively, showing that the continuum image is well centered at the origin of coordinates.

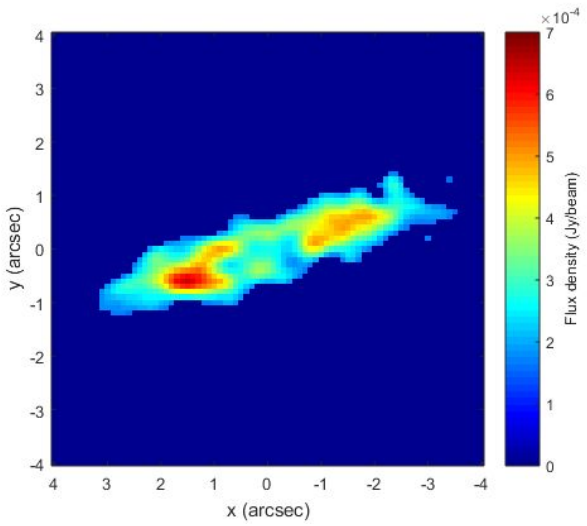

Figure 7. Sky map of the continuum flux density.

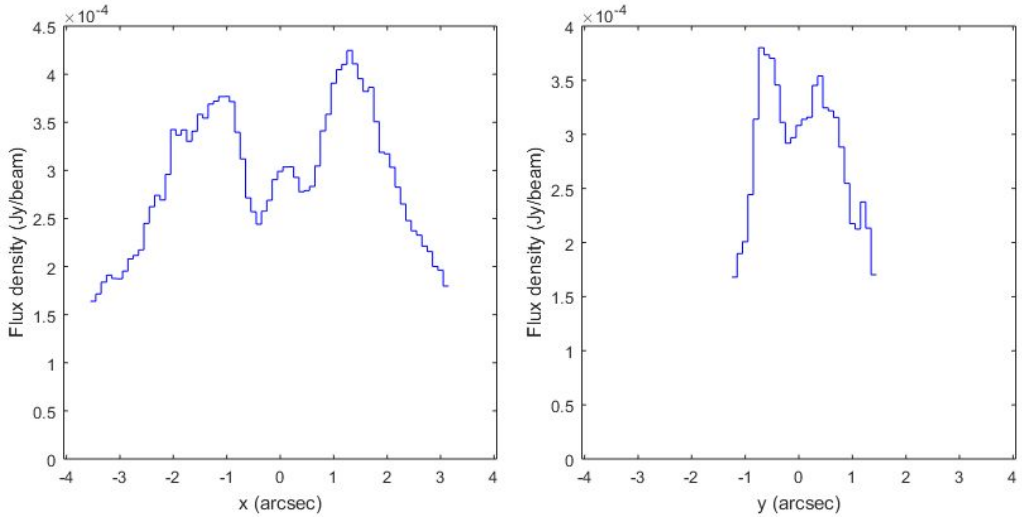

Figure 8. Projections of the continuum flux density on *x (left)* and *y (right)* axes averaged over pixels.

Figure 9 displays the dependence on angular distance, , and position angle φ (measured counter-clockwise from west) of the continuum flux density averaged over pixels exceeding 3σ. The tilt of the disc with respect to the *x* axis is seen to be between 15° and 20°. The continuum flux density is seen to extend further out than 4 arcsec, which would require a cut lower than 3σ to be studied.

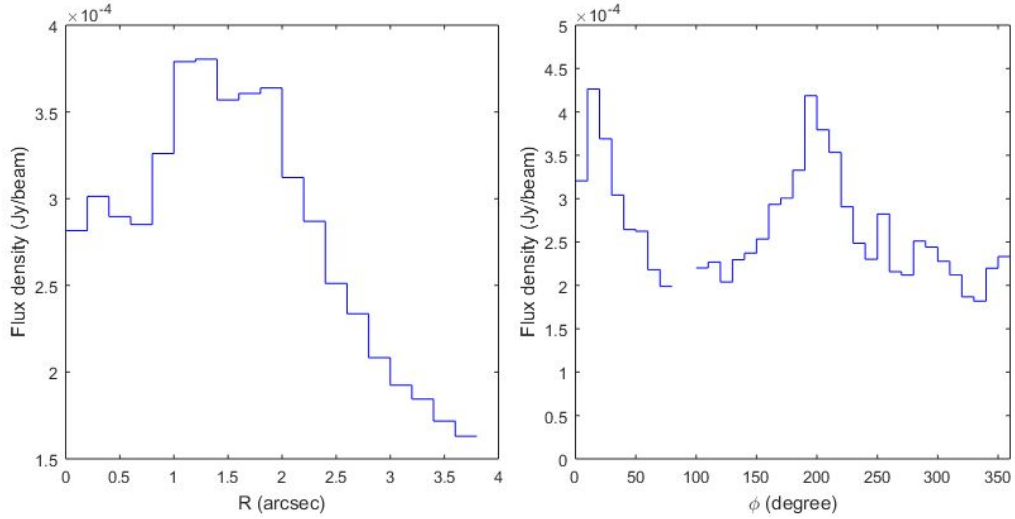

Figure 9. Dependence on R (*left*, note the zero offset on the ordinate axis) and φ (for $0.5'' < R < 2.5''$, *right*) of the continuum flux density averaged over pixels.

3.2. ***CO(3-2) data***

The data are presented in a grid of 360×360 pixels on the sky plane with pixel size of 0.1×0.1 arcsec^2 and 650 bins of Doppler velocity from −14.6 km/s to 19.8 km/s. The beam size is 0.50×0.38 arcsec^2 FWHM with PA=83.7°. The flux density distribution is shown in Figure 10 (left). The Gaussian fit gives a mean value of -1.74×10^{-4} mJy/beam and a σ of 8.8 mJy/beam. We use a 3σ cut for further analysis.

Figure 10 (right) displays the Doppler velocity spectrum, using as origin 2.78 km s^{-1} about which the profile is well symmetric. It shows a double-horn profile typical of a rotating volume. We restrict the velocity in the range of ±8.243 km/s about the origin.

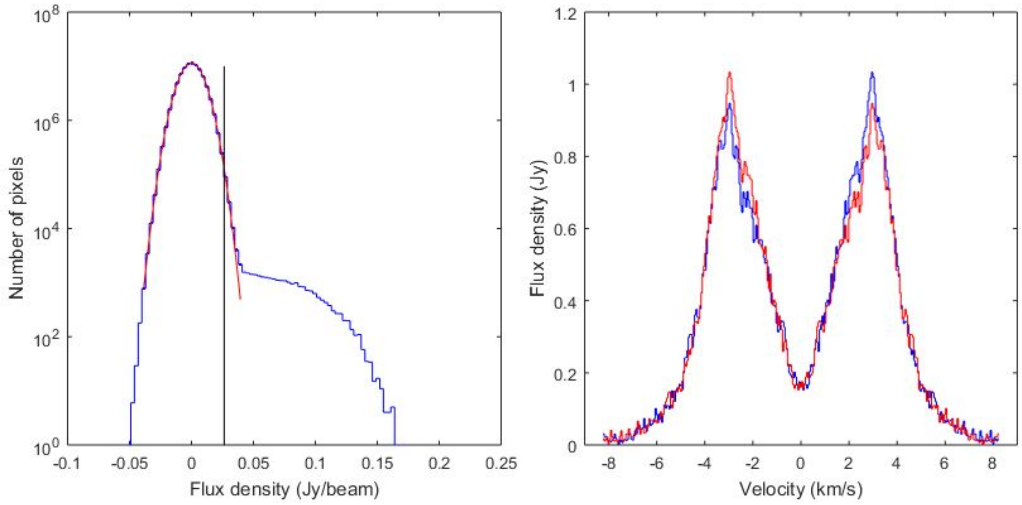

Figure 10. *Left:* Flux density distribution with the Gaussian fit (red curve), the vertical line shows the cut at 3σ. *Right:* Doppler velocity spectrum (blue). The red histogram is obtained by mirror symmetry about the origin.

The map of the line flux, integrated over Doppler velocities, F, is shown in Figure 11, together with its projections on the x and y axes averaged over pixels in Figure 12. The projected distributions are shown together with their reflections with respect to the origin. The mean values of the x and y projections are 0.0529 and −0.0090 arcsec respectively, showing that the source is also well centred at the origin of coordinates. However, small asymmetries can be seen at large distances from the centre in both x and y.

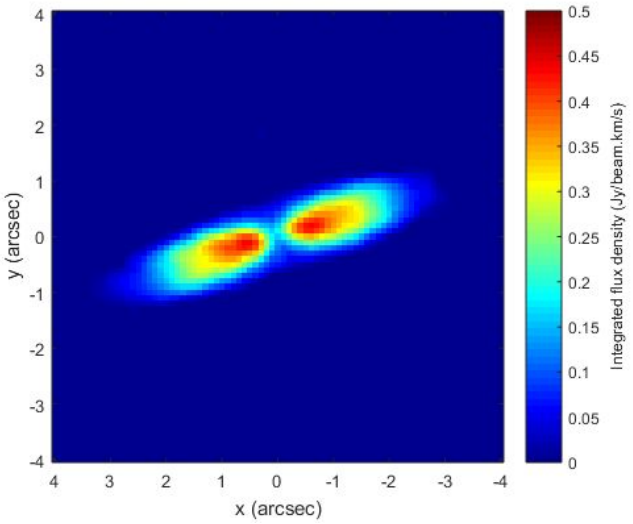

Figure 11. Sky map of the flux density integrated over Doppler velocities.

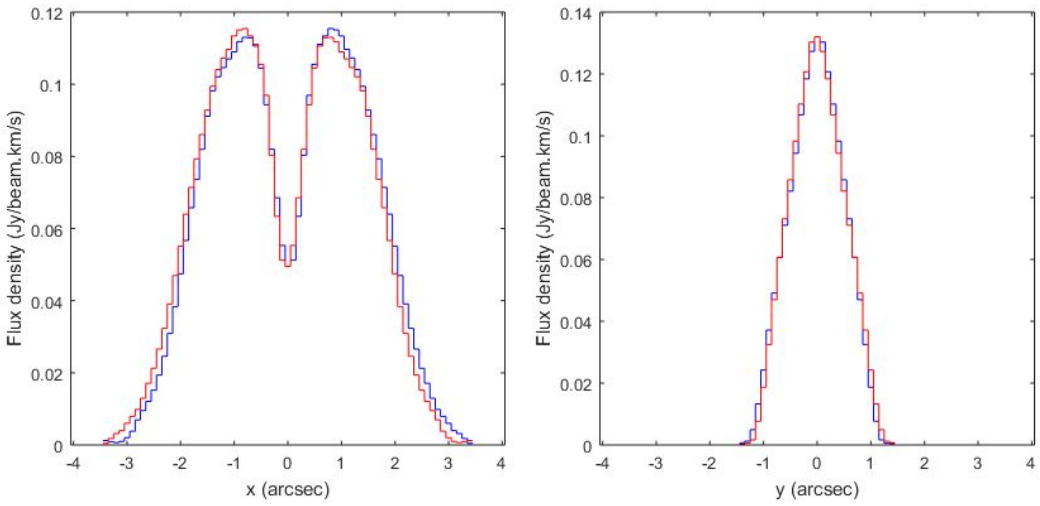

Figure 12. Distributions of the flux density integrated over Doppler velocities projected on x (*left*) and on y (*right*). The red histograms are obtained by mirror symmetry about the origin of coordinates.

Figure 13 shows the *R*-dependence of the integrated line flux. A two-Gaussian fit on the distribution gives R = 0.36 arcsec for the maximum flux. Contrary to the continuum distribution, the line distribution does not extend beyond 3 to 4 arcsec.

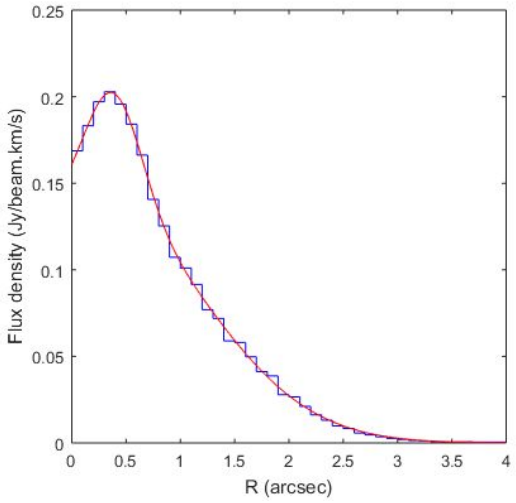

Figure 13. *R*-dependence of the line integrated flux averaged over pixels, together with the two-Gaussian best fit.

Figure 14 displays the sky map of the mean Doppler velocity, showing a clear east-west velocity gradient associated with the rotation of an edge-on disc about its axis. For the mean Doppler velocity hereafter, we apply an additional cut on the integrated line flux at 0.01 Jy beam^{-1} km s^{-1}.

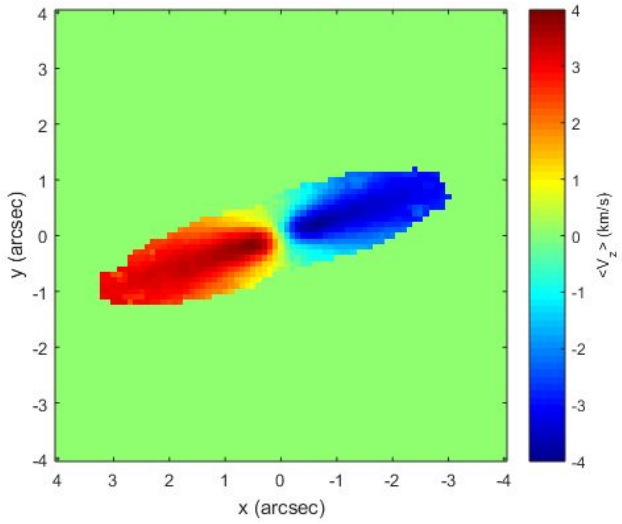

Figure 14. Sky map of the mean Doppler velocities.

Figure 15 (left) displays the dependence on position angle of the line flux averaged over pixels having R < 3 arcsec. Gaussian fits to the peaks in the line flux distribution give mean and sigma values of (18.5°, 13.1°) and (180° + 17.1°, 14.0°) respectively, which corresponds to a tilt of (18.5° +

17.1°)/2 = 17.8° of the disc plane with respect to the east-west direction. Close to the rotation axis, the averaged line flux nearly cancels.

The dependence on position angle of the mean Doppler velocity averaged in the same region is displayed in Figure 15 (right). It is well described by the form .

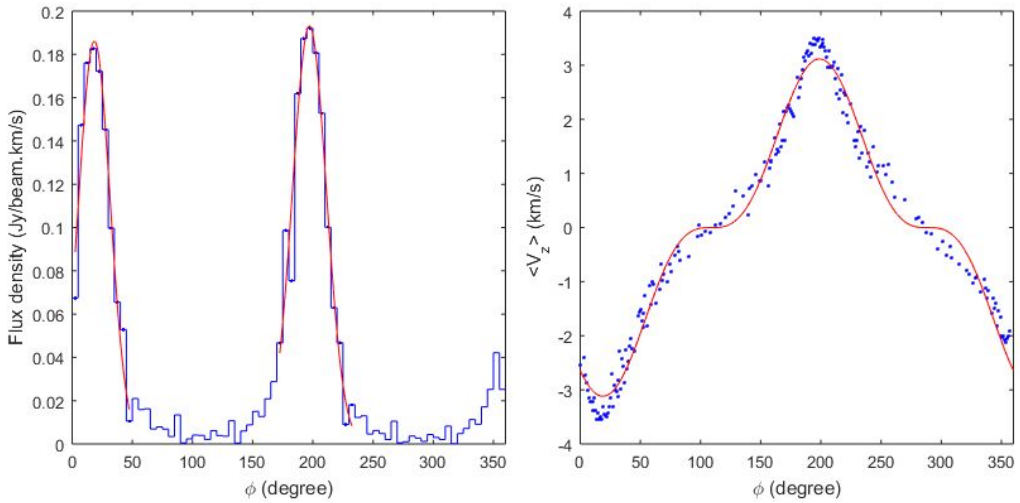

Figure 15. *Left:* Dependence on φ of the line integrated flux averaged over the region of R < 3″ with the 2 Gaussian fits (red curves). *Right:* Dependence on φ of the mean Doppler velocity average in the same region. The red curve is a fit of the form .

We define (*u,v*) coordinates obtained by rotation of 18º in the sky plane (about the *z* axis along the line of sight) of the (*x,y*) coordinates. Figure 16 displays the projections on *u* and *v* of the integrated flux averaged over pixels. A Gaussian fit to the *v*-projection gives a mean value of −0.001 arcsec and a σ of 0.308 arcsec. We apply a cut of 2σ (0.62 arcsec) on *v* for the *u*-projection.

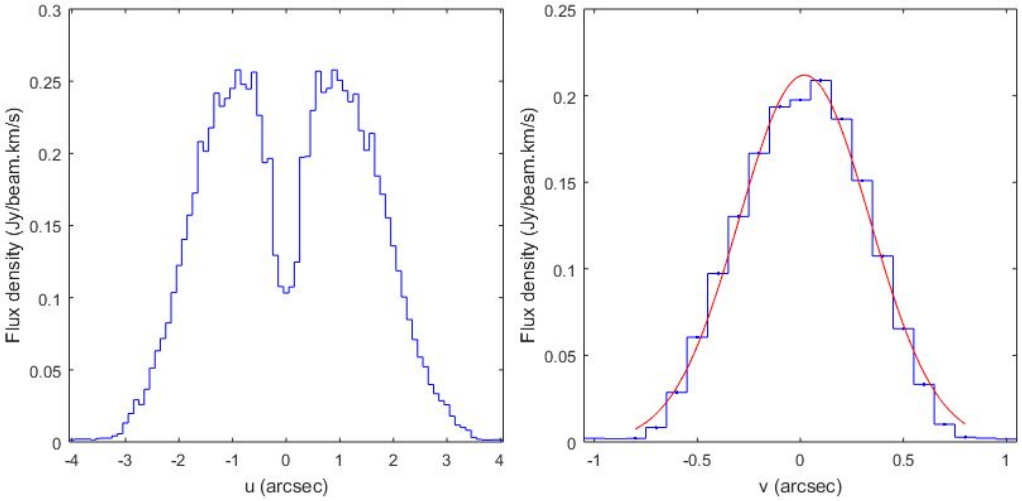

Figure 16. Distributions of the flux density integrated over Doppler velocities projected on *u* (left) and on *v* (right). In right panel, the red curve shows the Gaussian best fit.

Figure 17 shows the distribution of the mean Doppler velocity as a function of *u* for 3 different regions of *v*: $|v| < 0.2''$ (red), $0.2'' < |v| < 0.4''$ (green) and $0.4'' < |v| < 0.6''$ (blue). Here the average velocity is averaged over all pixels in the proper *u* bin and *v* interval, weighted by the integrated flux in each pixel. At large enough distances, the Doppler velocity is of the order of 3 km s^{-1}, with little dependence on *u*.

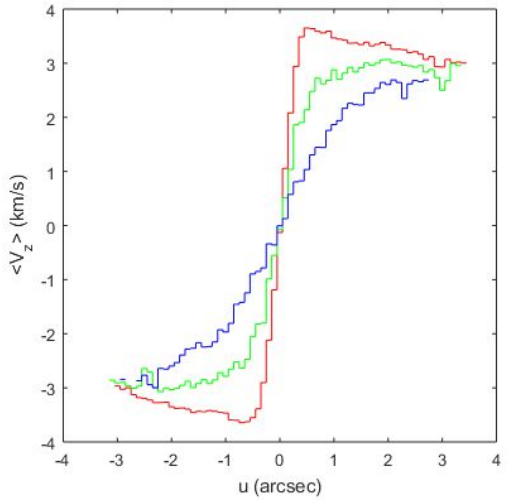

Figure 17. Distribution of mean Doppler velocity as a function of *u* for 3 different regions of *v*: $|v| < 0.2''$ (red), $0.2'' < |v| < 0.4''$ (green) and $0.4'' < |v| < 0.6''$ (blue).

Space distribution of the effective emissivity

We evaluate the effective emissivity from the values taken by the measured flux densities integrated over the velocity spectrum. We assume that the disc is very thin and obeys rotational symmetry around the *u* axis. It means that the effective emissivity ρ is a function of only , $v = 0$ by assumption. The effective emissivity then can be obtained simply by solving the integral equation where *F(u)* is the flux density integrated over the velocity spectrum at distance *u* to the rotation axis on the sky plane. The integral equation is solved by iteration, using as input 15 bins of *u* in steps of $0.2''$ from $0.5''$ to $3.5''$ and averaging the flux over $|v| < 0.31''$. Integration along the line of sight is made in steps of *z* of $0.01''$ from $-3.5''$ to $3.5''$. The effective emissivity is defined in 15 *r* bins of $0.2''$ from $0.5''$ to $3.5''$. The iterative process is stopped when the difference between observations and fluxes obtained by integration of the effective emissivity along the line of sight reaches a value of 5‰. Figure 18 compares the *u* measured and modelled distributions of *F(u)*, giving evidence for the effectiveness of the iterative process. Also shown is the obtained distribution of $\rho(r)$ that displays a nearly flat profile in the centre, up to ~2 arcsec, before decreasing steeply and cancelling at ~3.5 arcsec.

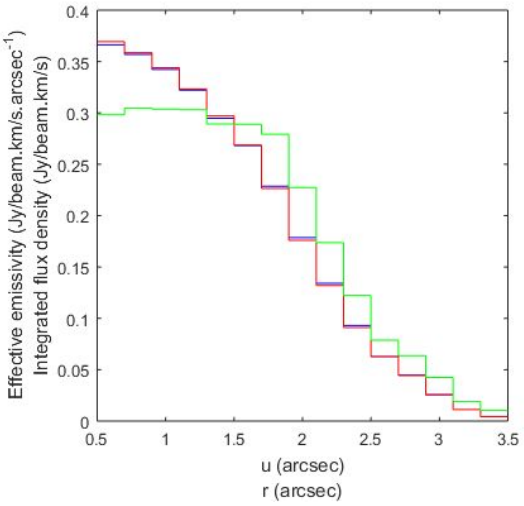

Figure 18. Comparison of the *u* distributions of the flux density for the data (blue) and the model (red). The *r* distribution of the effective emissivity ρ is shown in green (in units of Jy beam^{-1} km s^{-1} arcsec^{-1}).

III. CONCLUSION

In summary, the source of CO(3-2) emission of 49 Cet has been shown to be a disc, of thickness 0.7 arcsec FWHM, perpendicular to the sky plane and making an angle of ~18° with respect to the east-west direction. The effective emissivity has been calculated in space under the hypothesis of rotational invariance about the disc axis. It is nearly constant at distances between 0.5 and ~2 arcsec from the star before decreasing steeply and cancelling at ~3.5 arcsec. The thickness of the disc is ~0.7 arcsec FWHM. The next step would be to calculate the *r* and *v* dependences of the rotation velocity under the same hypothesis but the short time imparted to the internship prevented me to do so. Continuum observations have been analysed, also displaying a disc structure, extending however to larger radii than for the line.

BIBLIOGRAPHY

Dent, W. R. F., Greaves, J. S., & Coulson, I. M. 2005, MNRAS, 359, 663

Dent, W. R. F., Wyatt, M. C., Roberge, A., et al. 2014, Sci, 343, 1490

Greene, T. 2001, American Scientist, 89, 316

Hughes, A. M., Wilner, D. J., Kamp, I., & Hogerheijde, M. R. 2008, ApJ, 681, 626

Moor, A., Abraham, P., Juhasz, A., et al. 2011, ApJ, 740, L7

Rhee, J., Song, I., Zuckerman, B., & McElwain, M. 2007, ApJ, 660, 1556

Roberge, A., Kamp, I. , Montesinos, B. et al., 2014, ApJ, 771, 69

Siess, L., Dufour, E., & Forestini, M. 2000, A&A, 358, 593

Thi, W. F., et al. 2001, ApJ, 561, 1074

Torres, C., Quast, G., Melo, C., & Sterzik, M. 2008, in Handbook of Star Forming Regions, Volume II: The Southern Sky, ed. Bo Reipurth (ASP Monograph Publication, Vol. 5; San Francisco, CA: ASP), 757

van Leuween, F. 2007, A&A, 474, 653

Vietnam National Satellite Center. 2016, Department of Astrophysics (Hanoi: VNSC), https://vnsc.org.vn/en/about-vnsc/department-of-astrophysics/

Williams J. P., Cieza L. A., 2011, ARA&A, 49, 67

Zuckerman, B. & Song, I., 2012, AJ, 758, 77

Zuckerman, B., Forveille, T., & Kastner, J. H. 1995, Nature, 373, 494